Electronic Supplementary Material (ESI) for ChemComm.
This journal is © The Royal Society of Chemistry 2017

Supporting Information for

Naphthalene-fused Dimer of an Anti-aromatic Expanded Isophlorin

Baddigam Kiran Reddy,[‡,1] Jeff Rawson,[‡2,3] Santosh C. Gadekar,[1] Paul Kögerler,[*,2,3] and Venkataramanarao G. Anand[*,1]

1. Department of Chemistry, Indian Institute of Science Education and Research, Pune 411008, India
2. Peter Grünberg Institute 6, Forschungszentrum Jülich, 52428 Jülich, Germany
3. Institute of Inorganic Chemistry, RWTH Aachen University, 52074 Aachen, Germany

Contents

Synthetic details

General methods

All reagents and solvents were of commercial reagent grade and were used without further purification except where noted. Dry CH_2Cl_2 was obtained by refluxing and distillation over P_2O_5. Synthesis was carried out under an inert atmosphere using standard Schlenk line techniques. NMR spectra were recorded on a JEOL 400 MHz and BRUKER 400 MHz spectrometers. Chemical shifts (δ) are reported in parts per million (ppm). Tetrathienylethene[1] and trithienyldimethane **8**[2] were synthesized as previously described.

Synthetic procedure for **6**

A mixture of tetrathienylethene, (178 mg, 0.5 mmol), **5**, and trithienyldimethane diol, **4**, (820 mg, 1 mmol) was stirred in 100 mL of dry dichloromethane. The solution was purged with argon for 10 min. and shielded from light. $BF_3.OEt_2$ (60μL, 0.5 mmol) was added and stirring continued for 2h. After adding ten equivalents of $FeCl_3$ under open atmosphere, the mixture was stirred for an additional two hours. The reaction mixture was passed through a short basic alumina column. This mixture was purified by recrystallization from dichloromethane. **6** was obtained as a metallic green solid (100mg, 10.4% yield).

UV-vis (THF): $\lambda_{max}(\varepsilon)$: 554(101176). **MALDI-TOF** m/z: Calcd. for $C_{98}H_{36}F_{20}S_{10}$: 1911.9705; observed: 1911.7206 (100.0%, M+). **Crystal data:** C_{99} H_{37} Cl_3 F_{20} S_{10} (Mr = 2033.23), Triclinic, space group P-1 (no. 2) , a = 15.552(3) Å, b = 17.106(3) Å, c = 20.345(4) Å, α = 109.332(4)° β = 104.391(4)° γ = 96.259(4)°, V = 4837.3(15) $Å^3$, Z = 2, T = 100(2) K , D_{calcd} = 1.396mg cm^{-3}, R_1 = 0.1198 (I>2s(I)), R_w (all data) = 0.2465, GOF = 1.143.

Precursor Synthesis

Scheme S2. Synthetic route to the trithienyldiol **4**.

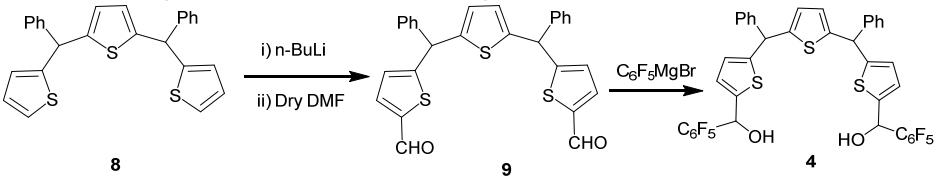

8 9 4

5,5'-Trithienyldimethane-2,2'-dicarbaldehyde (9)

To a stirred solution of trithienyldimethane **8** (0.5 g, 1.1 mmol) in dry ether (15mL) was added n-butyl lithium (2.5 M in hexane, 1.91ml, 4.8 mmol). Dimethylformamide (0.37ml, 4.8 mmol) in 3 mL dry ether was added dropwise with stirring at room temperature, and stirring was continued for a further 2h. The mixture was washed successively with water; dilute hydrochloric acid, water, and sodium bicarbonate solution, dried and evaporated. The residue was purified by column chromatography (Silica gel 100-200 mesh) to give **9** as an orange residue (0.34 g., Yield: 61%).

5,5'-Trithienyldimethane-2,2'-bis(perfluorophenyl)dicarbinol (4)

To a stirred solution of trithienyl dialdehyde **9** (1.1 mmol, 0.746 g in 15 ml THF) under argon atmosphere at 0 °C, freshly prepared Grignard reagent (C_6F_5MgBr, 2.7 mmol) was added. Stirring

continued for 2 hrs while the reaction mixture was allowed to gradually warm to room temperature, and the reaction was then quenched with saturated NH_4Cl solution. The mixture was extracted with ether and the combined organic layers were washed with water and brine solution. After drying over Na_2SO_4, the solvents were removed under vacuum and the residue was purified by column chromatography (silica gel 100-200 mesh) to yield the pure diol **4** as a brown residue (0.9 g, Yield: 41%).

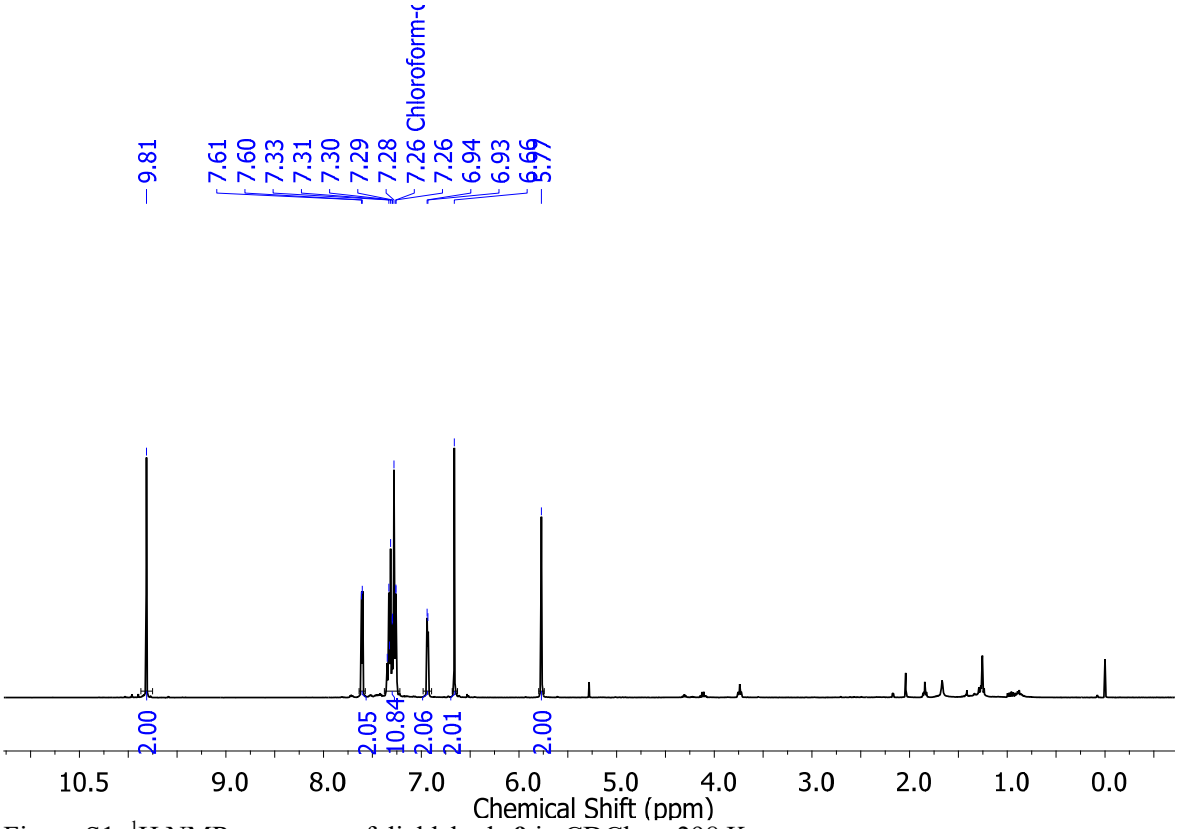

Figure S1. ^{1}H NMR spectrum of dialdehyde **9** in $CDCl_3$ at 298 K.

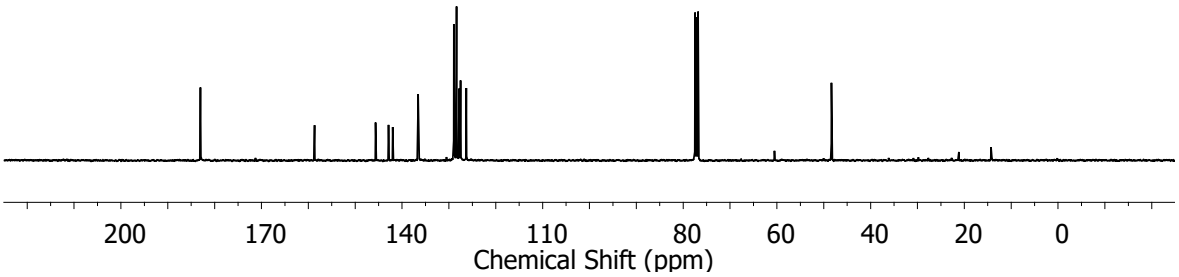

Figure S2. 13C NMR spectrum of dialdehyde **9** in CDCl3 at 298 K.

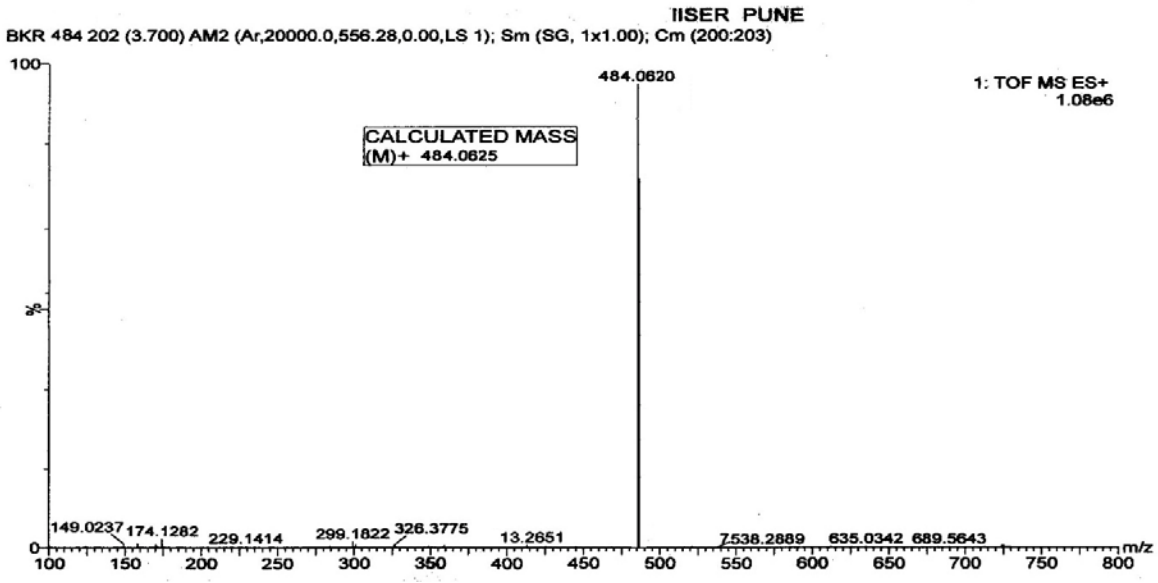

Figure S3. HR-ESI TOF spectrum of dialdehyde **9.**

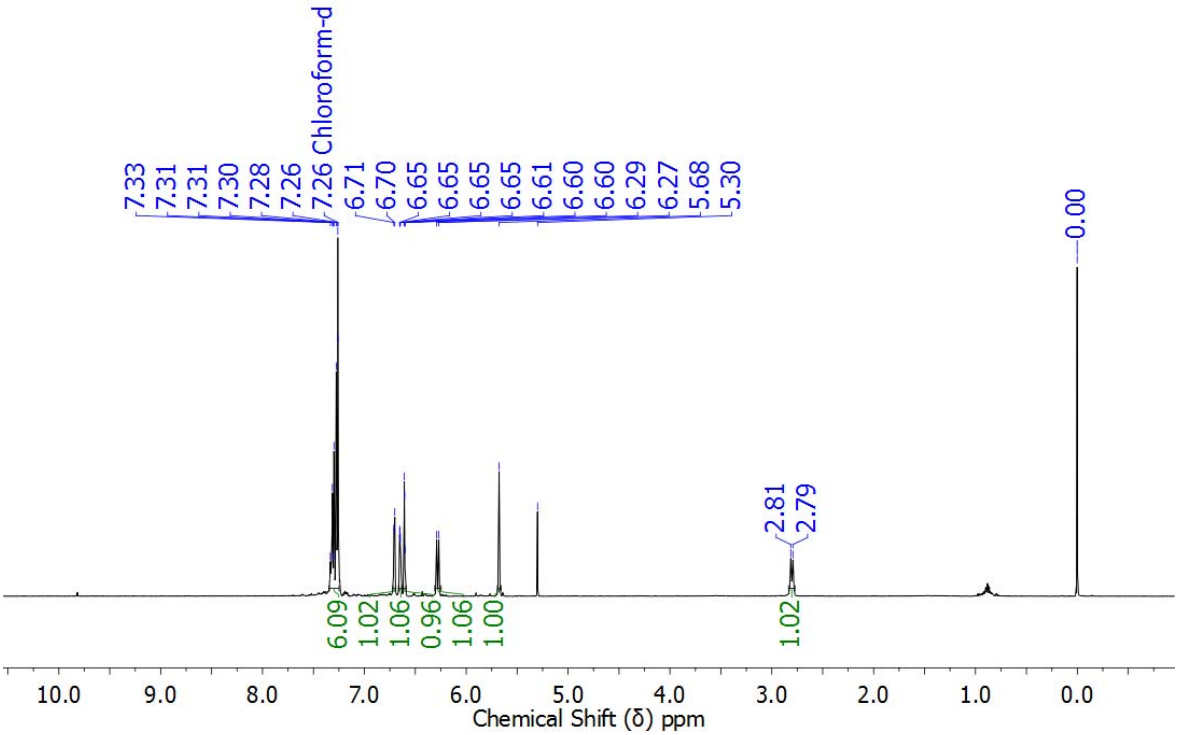

Figure S4. ^{1}H NMR spectrum of diol **4** in $CDCl_3$ at 298 K.

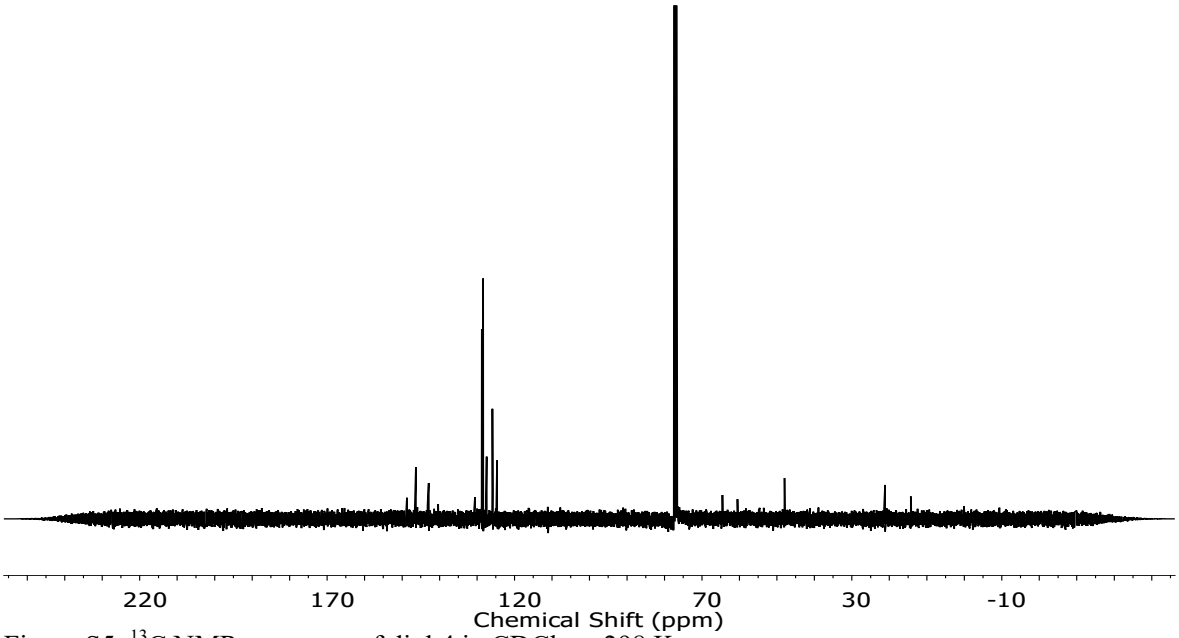

Figure S5. ^{13}C NMR spectrum of diol **4** in $CDCl_3$ at 298 K.

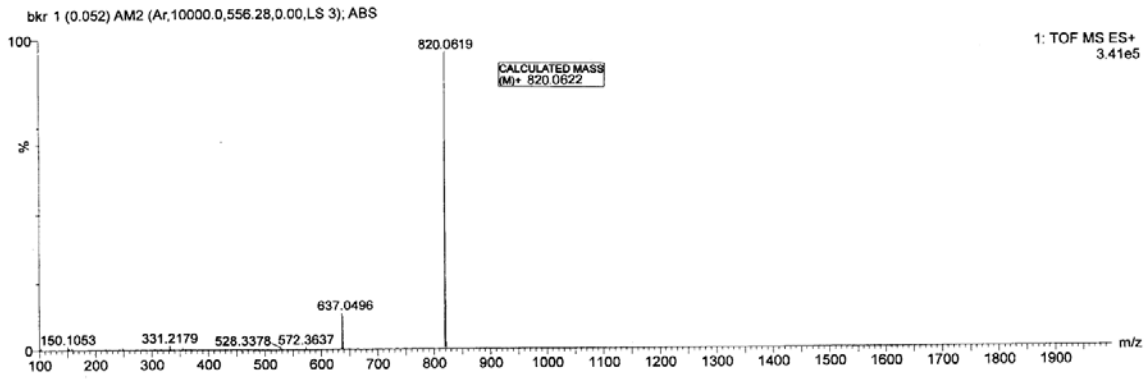

Figure S6. HR-ESI TOF spectrum of diol **4**.

Spectroscopic Details

Instrumentation and sample preparation

Proton and fluorine NMR spectra of 6 were collected in chlorobenzene solvent at 400 K on a Bruker Avance 600 MHz NMR spectrometer equipped with a CryoProbe™ Prodigy. Sample holders were Wilmad Precision fused quartz 600 MHz tubes, Chlorobenzene-d_5 was supplied by Alfa Aesar, and trichlorofluoromethane was supplied by Sigma Aldrich. The ^{19}F spectrum and its assignment are presented as Figure S7, and the ^{1}H spectrum as Figure S8.

Mass spectra of the **6** compound were obtained by dissolving a small portion in a few drops of tetrahydrofuran; this was mixed in a 1:1 ratio with a solution of the HABA matrix (hydroxyazobenzoic acid, 10 mg/mL). Small droplets (~1 μL) were deposited on a stainless steel target plate and allowed to dry under ambient conditions. High resolution orbitrap mass spectra were acquired using a MALDI-LTQ-Orbitrap XL mass spectrometer (Thermo). Automatic gain control was used, and two laser sweep shots were applied before spectrum acquisition. A high resolution mass spectrum and isotopic analysis are presented as Figure S9.

Electronic absorption measurements were collected using a Perkin Elmer Lambda-950 spectrophotometer (for quantitative measurements in chlorobenzene) or a Specord 600 from AnalytikJena (qualitative measurements in toluene). Sample cuvettes were 10 mm pathlength quartz Suprasil cells from Hellma Analytics, toluene was Chromasolv grade from Sigma Aldrich, and chlorobenzene was 99% from Alfa Aesar.

To ensure complete dissolution, solutions were sonicated for ten minutes, warmed with a heat gun, and then allowed to return to room temperature. Solutions at final spectroscopic concentration were added to cuvettes through 200 μm Teflon syringe filters. For quantitative absorption measurements in chlorobenzene, a precision of only about ± 20% could be achieved due to the low quantity of pure material available and difficulties with its complete dissolution. The spectrum measured in toluene is presented as Figure S10, and that in chlorobenzene as Figue S11. Details of the spectral deconvolution are provided with Figure S12, and integrations for determination of oscillator strengths are provided in Figure S13.

Single-crystal X-ray diffraction analysis data were collected at 100K with a Bruker D8 Venture Duo X-ray diffractometer equipped with Microfocus X-ray source (operated at 50 W; 50 kV/1 mA), graded multilayer optics for monochromatic (λ = 0.71073 Å) focused X-ray beam and Photon 100 CMOS chip based detector system. The studied crystal was grown by slow evaporation of a chloroform solution containing a few drops of trifluoroacetic acid. One molecule of chloroform per **6** molecule was included in the unit cell.

NMR spectra

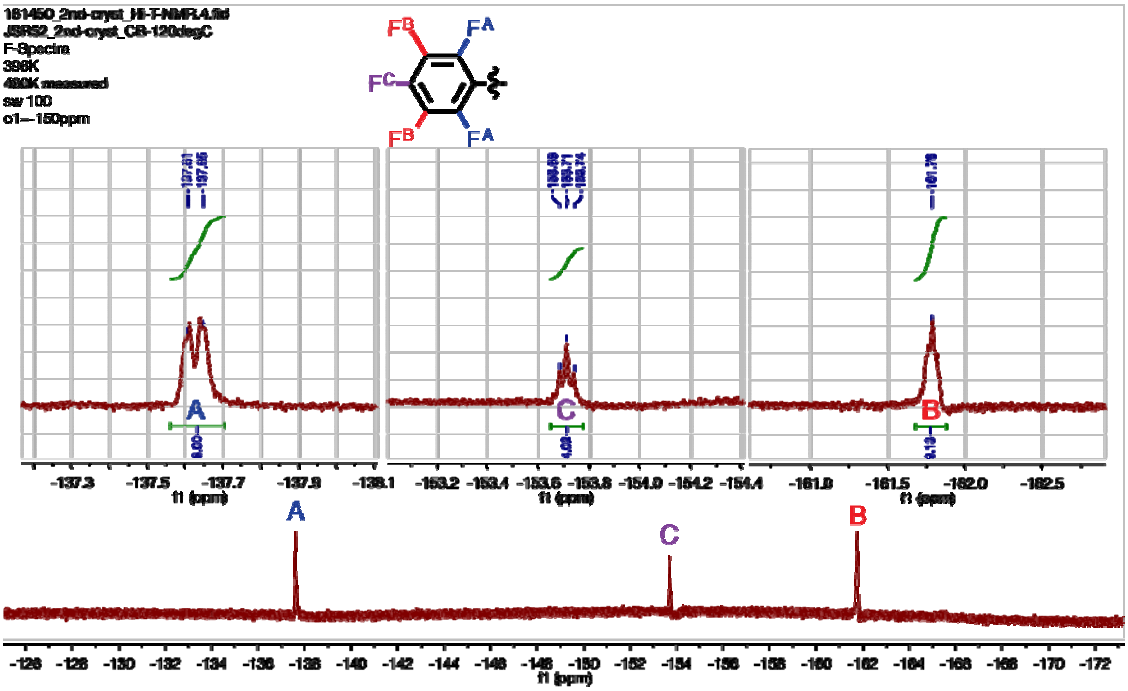

Figure S7. Fluorine NMR spectrum of **6** measured at 564.46 MHz in chlorobenzene-d_5 solvent at 400 K. Chemical shifts are referenced to $CFCl_3$ (= 0.00 ppm, not shown). δ(ppm): 137.58-137.67 (dd, 8F, *J* = 23, 7 Hz); 153.67-153.75 (pentuplet, 4F, *J* = 7 Hz); 161.78 (ttd, 8F, *J* = 7,7,1 Hz). Noise, shimming, and phasing problems complicated the solution of this NMR spectrum, but the tentative assignments noted here have been derived by comparing the results from rephasing, baseline correction, and multiplet analysis tools in MNova and also comparing between other spectra of the compound when it was less pure. The coupling of ~1 Hz for fluorine B is to a proton at a neighboring thiophene β-position.

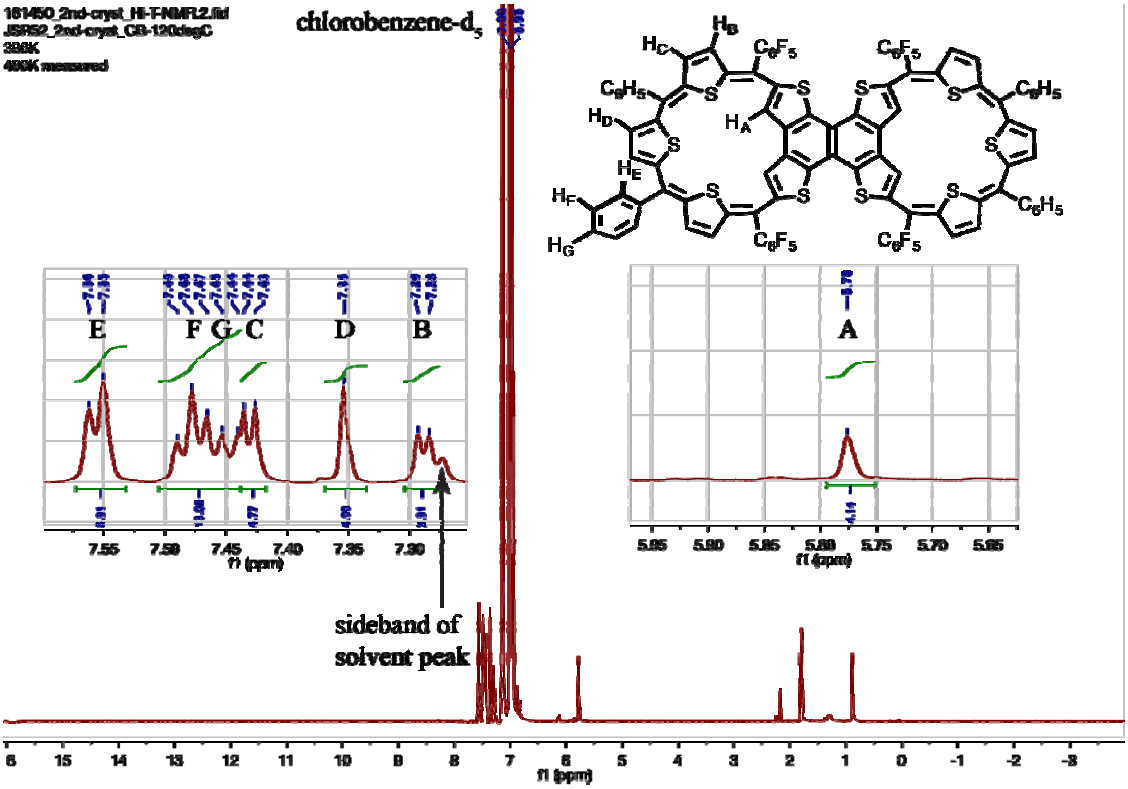

Figure S8. Proton NMR spectrum of **6** measured at 600 MHz in chlorobenzene-d_5 solvent at 400 K. Chemical shifts are referenced to those of residual solvent protons. δ(ppm): 7.556 (d, 8H, J = 6.9 Hz); 7.490-7.441 (m, 12H); 7.431 (d, 4H, J = 5.7 Hz); 7.354 (s, 4H); 7.289 (d, 4H, J = 5.7 Hz); 5.776 (s, 4H). The key features that buttress these assignments are the apparent downfield shift of aryl proton E due to its location in the shielding region of nearby aromatic groups, the partially-resolved $J_{1,4}$ couplings of aryl protons in the multiplet, and the apparent broadening of proton B due to its unresolved through-space coupling to a fluorine nucleus of the proximal perfluoro(phenyl) ring.

Mass Spectrum

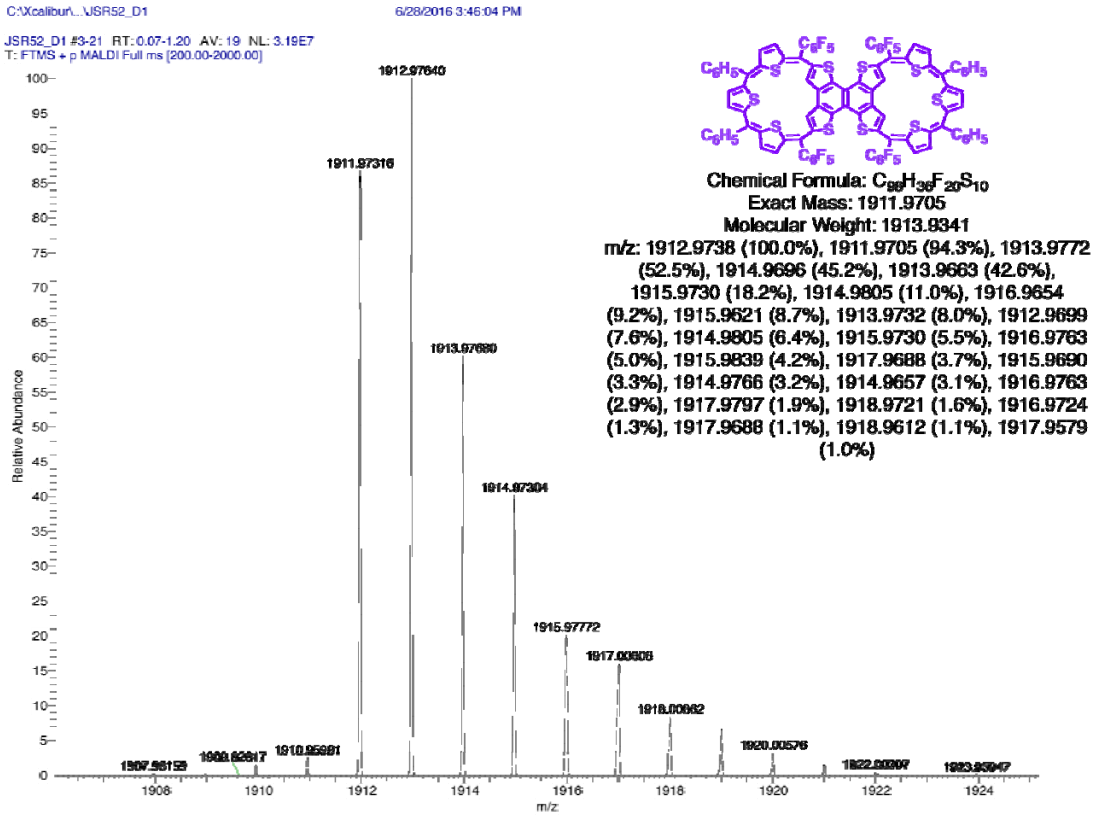

Figure S9. High resolution mass spectrum of **6** compound ionized from HABA matrix. In the top right is provided the expected peak intensities calculated by ChemDraw software (Perkin Elmer).

Electronic absorption spectra

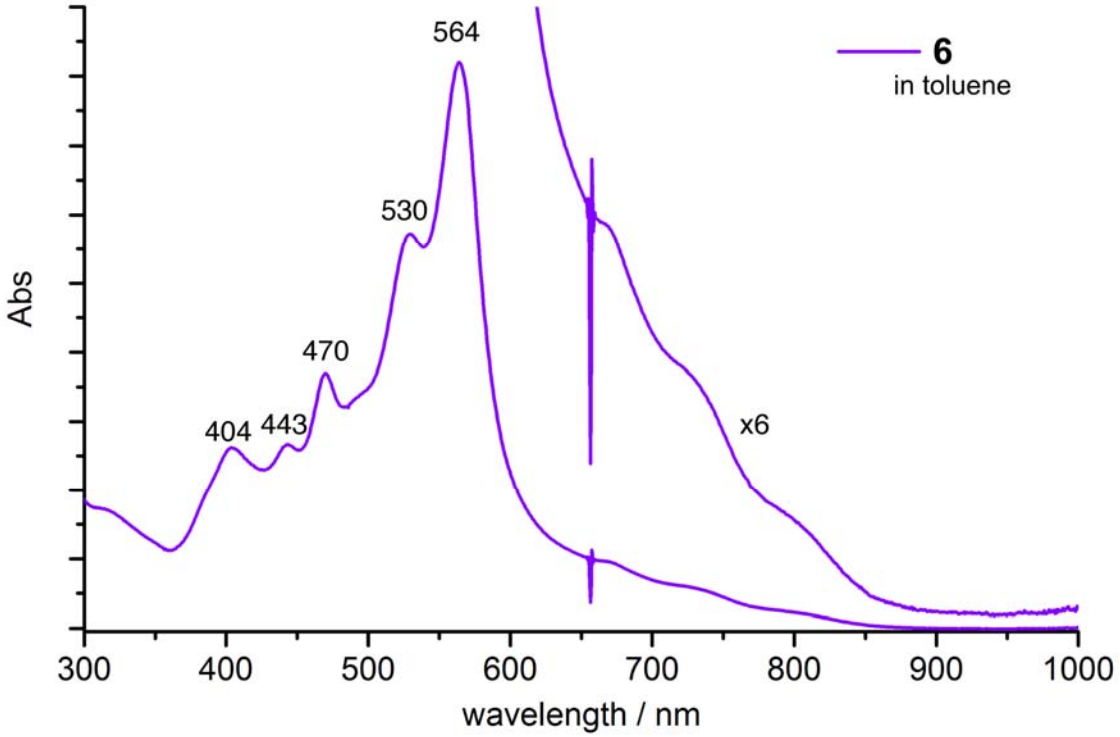

Figure S10. Electronic absorption spectrum of **6** in toluene solvent. A second trace at ×10 intensity is provided for the wavelength range from 625–100 nm. Note that peak maxima differ from those measured in chlorobenzene by 3 nm or less.

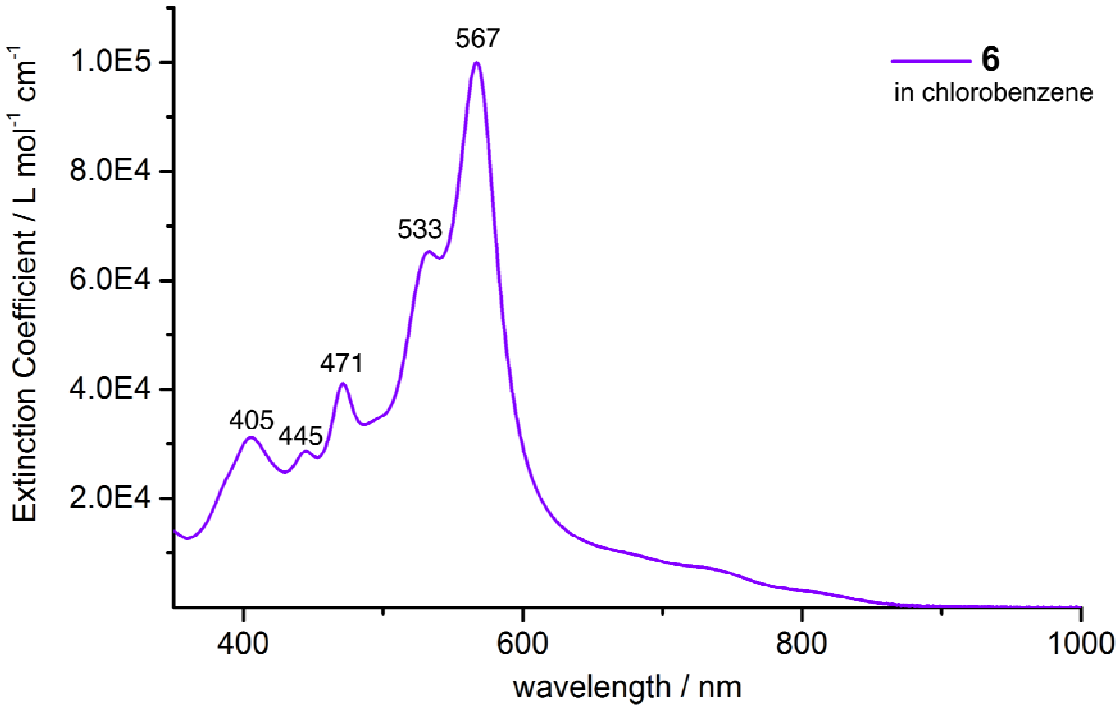

Figure S11. Electronic absorption spectrum of **6** in chlorobenzene solvent.

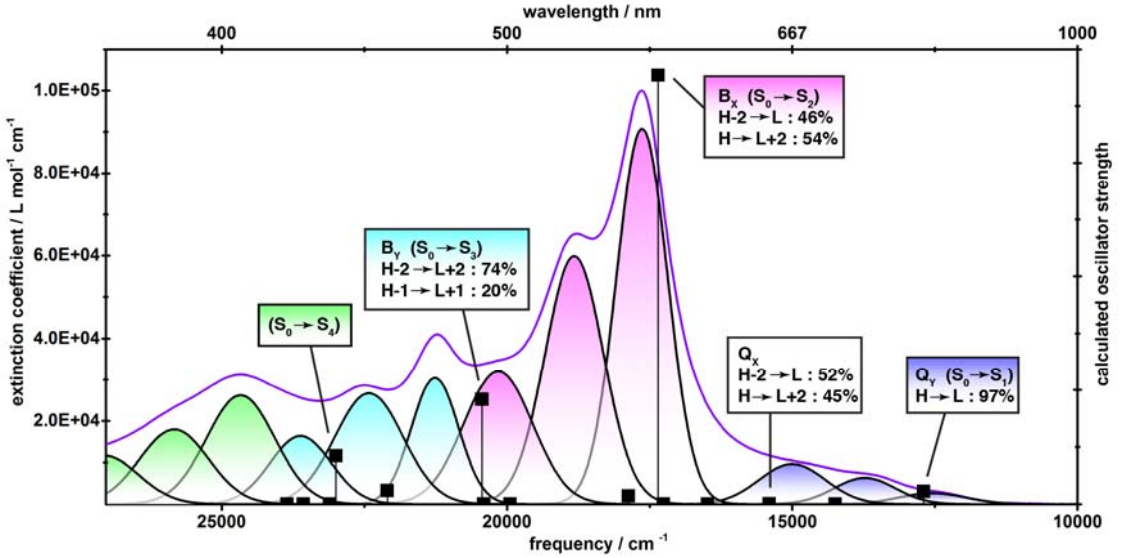

Figure S12. Expansion of the deconvoluted spectrum provided in the main text. Note that with the twelve Gaussian curves shown, this model of the spectrum is not unique; it is a guide regarding likely divisions of the spectrum into the four principle electronic manifolds. Not shown here is an additional curve used to account for additional spectral broadening.

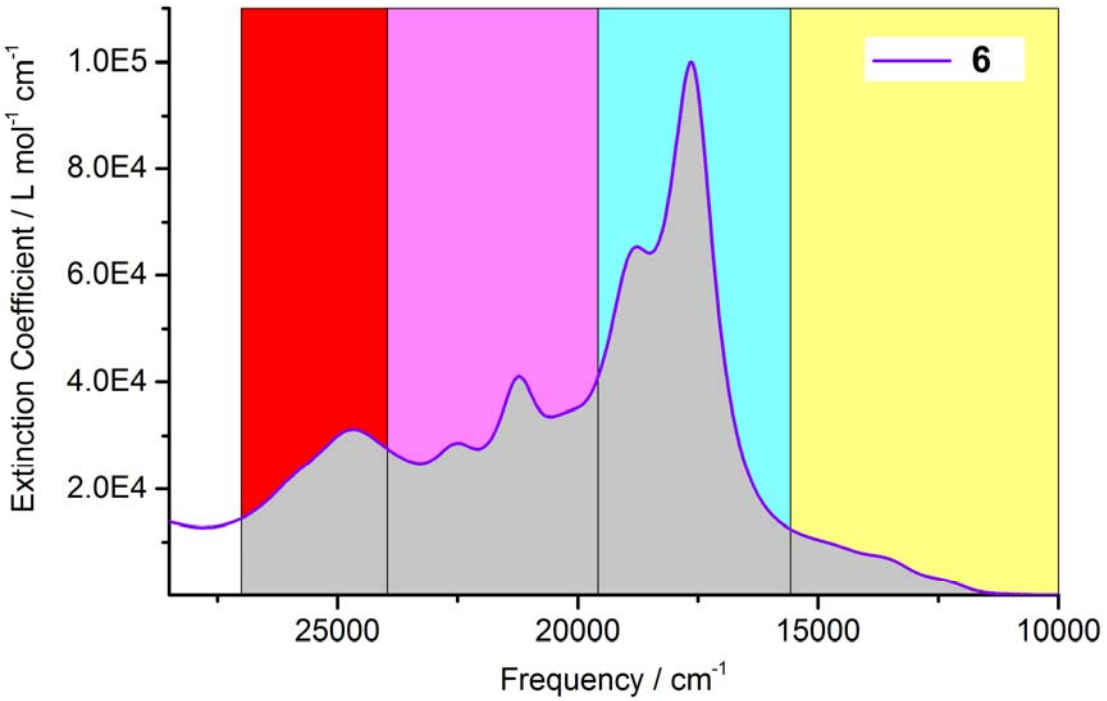

Figure S13. Regions of integration for the determinations of oscillator strengths for the four principle visible-range electronic transitions of **6**. As noted above, a unique model for subdividing the spectrum cannot be achieved and thus these lines are subjective. Oscillator strengths are: $f(S_0 \rightarrow S_1,$ 10000–15574 $cm^{-1}) = 0.112$; $f(S_0 \rightarrow S_2,$ 15574–19580 $cm^{-1}) = 0.914$; $f(S_0 \rightarrow S_3,$ 19580–23961 $cm^{-1}) = 0.596$; $f(S_0 \rightarrow S_4,$ 23961–27000 $cm^{-1}) = 0.324$.

X-ray crystal structure

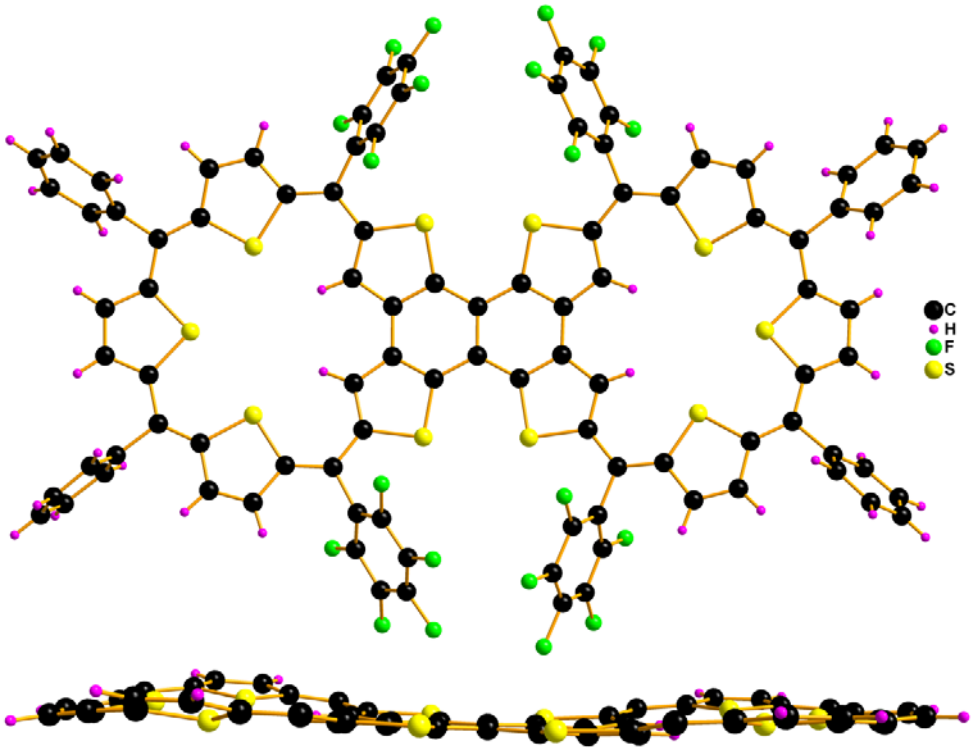

Figure S14. Face-on and edge-on views of the structure of **6** determined by single-crystal X-ray diffraction.

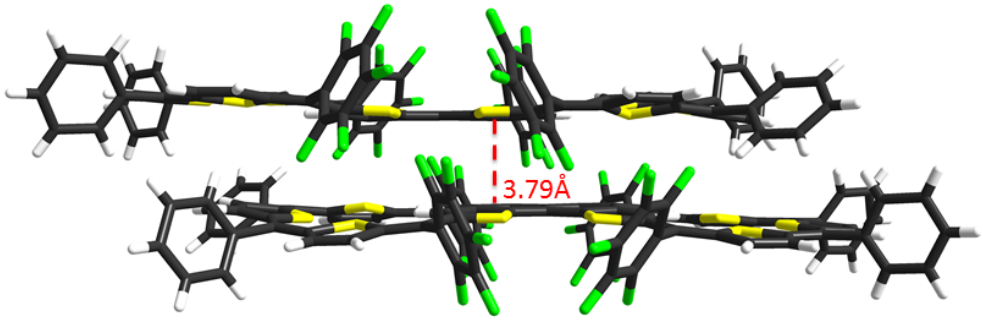

Figure S15. Offset π-π stacking in the crystallographically-determined molecular structure of **6**.

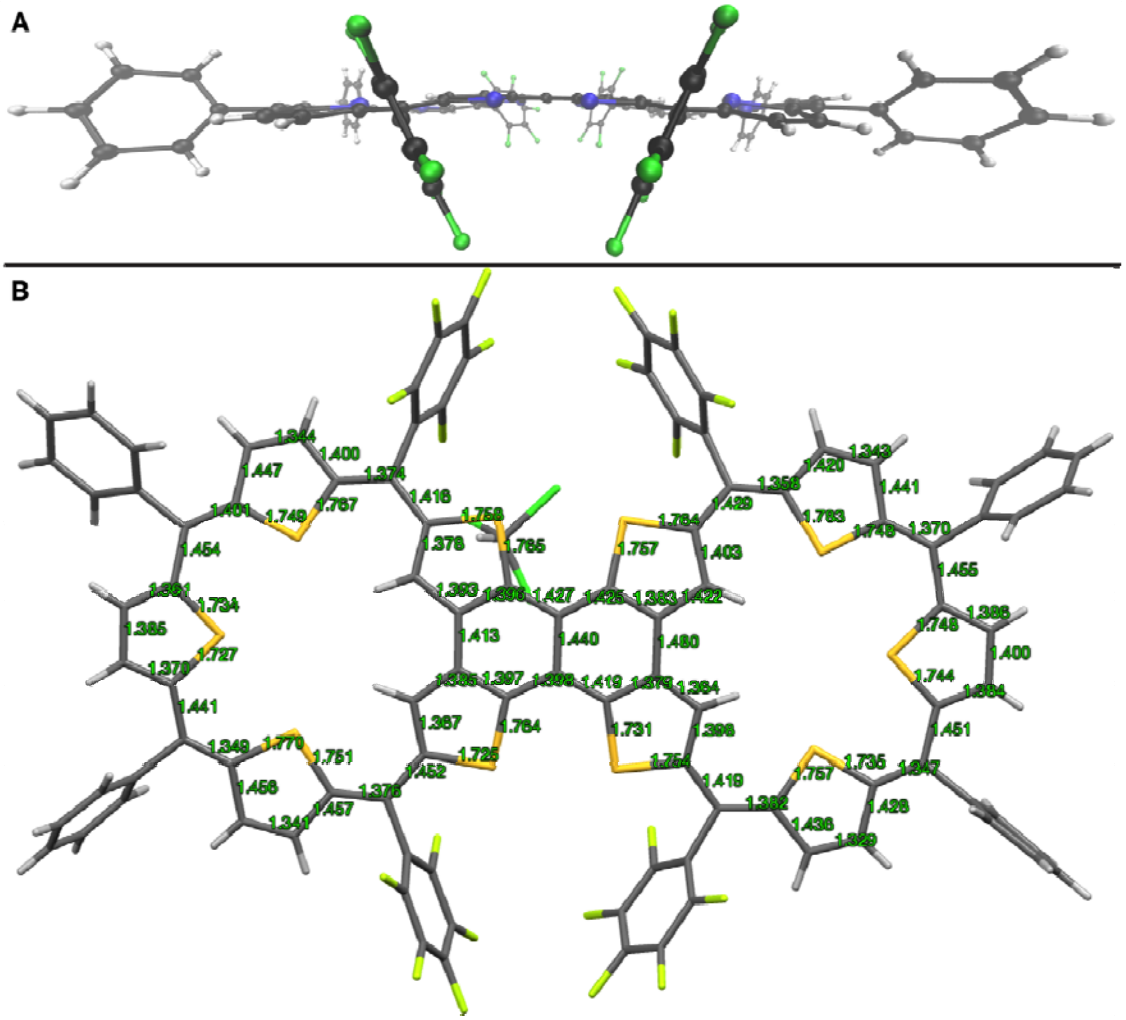

Figure S16. (A) Edge-on perspective view of the structure determined by single-crystal X-ray diffraction for **6**. (B) Face-on view of the structure determined by single crystal x-ray diffraction for **6**, with the molecule of chloroform solvent included in the crystal. The lengths of all heavy atom bonds in the 60-atom bimacrocyclic skeleton are indicated in Ångstroms.

Computational Details

Software packages

Density functional theory (DFT) calculations, including magnetic shielding calculations to determine NICS(1) values,[3] were performed using Gaussian09 Rev. D.01 software package,[4] aided by the Gaussview 5 visualization and front-end program.[5] All calculations employed the integral equation formalism variant of the polarizable continuum model to simulate solvation effects, with toluene as the solvent (SCRF=IEFPCM); tight SCF convergence parameters and an ultrafine integration grid were used (scf=tight, int=grid=ultrafine). The result files of time-dependent DFT (TDDFT) calculations were parsed, and their population analyses constructed, using Gausssum,[6] and publication-quality images of molecular structures determined from calculations and crystallography were produced using VMD.[7] Partitioning of the electron densities into sigma and pi contributions, calculation of Localized Orbital Locator[8] 2-dimensional and 3-dimensional datasets, and critical point analyses were accomplished using Multiwfn.[9]

Structural simplifications, functionals, and basis sets

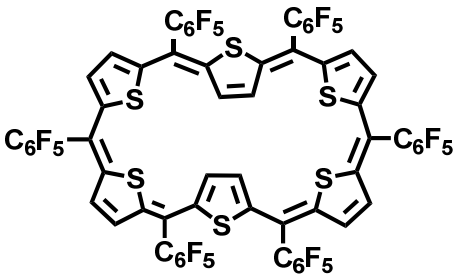

S6

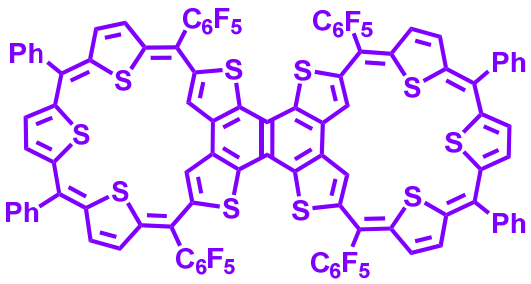

6

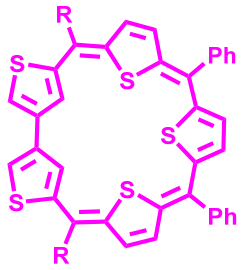

Thiasapphyrinoid 7

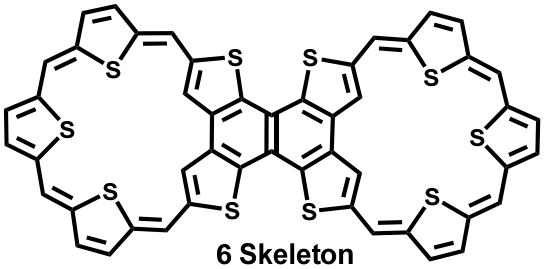

6 Skeleton

The structures of all compounds were simplified to the D_{2h} point group, which reduced the computational demand of calculations while also affording unambiguous assignments of axes, irreducible representations, etc. Macrocycle skeleton atoms were all allowed to lie in a single plane. For all phenylated and perfluorophenylated compounds, aryl rings were twisted to dihedral angles of 90° with respect to the plane of the macrocyclic cores. The unambiguous segmentation of the electron density into orthogonal sigma and pi components required truncation of the (perfluoro)phenyl rings, so that only the **6** skeleton structure was considered without reoptimization after this simplification. Frontier orbital wavefunctions of this structure are compared with those for the full **6** compound in Figure S23. The correlation diagram was constructed by generating new input files in which either the ethylene bridge or the remainder of

the molecule were deleted, also without structural reoptimization but using hydrogen atoms at default bond lengths to satisfy the open valences this created.

Functional choice was initially explored using the known **S6** compound[10] as a test case. All structures were optimized using the CAM-B3LYP[11] functional as implemented in Gaussian09 Rev. D.01, and the 6-311G all-electron basis set with two added d functions (6-311g(2d)).[12] For TDDFT calculations, several hybrid exchange-correlation functionals were While range separation is often useful for modeling the linear response of large conjugated molecules, for these compounds we found that the M11[13] and CAM-B3LYP functionals both gave substantial deexcitation terms in the lists of configurations for each transition. Our best results were found with the Becke three- parameter hybrid[14] and the Lee-Yang-Parr correlation functional[15] (B3LYP).

Basis sets for some calculations were truncated. To meet computational demands, the TDDFT calculations on the **6** compound needed to employ a diminished basis set where S and C atoms had the 6-311G(d) set and H and F atoms had the 6-31G set. This basis set was used for the remaining calculations involving **6**, such as LOL and correlation diagram.

NICS calculations

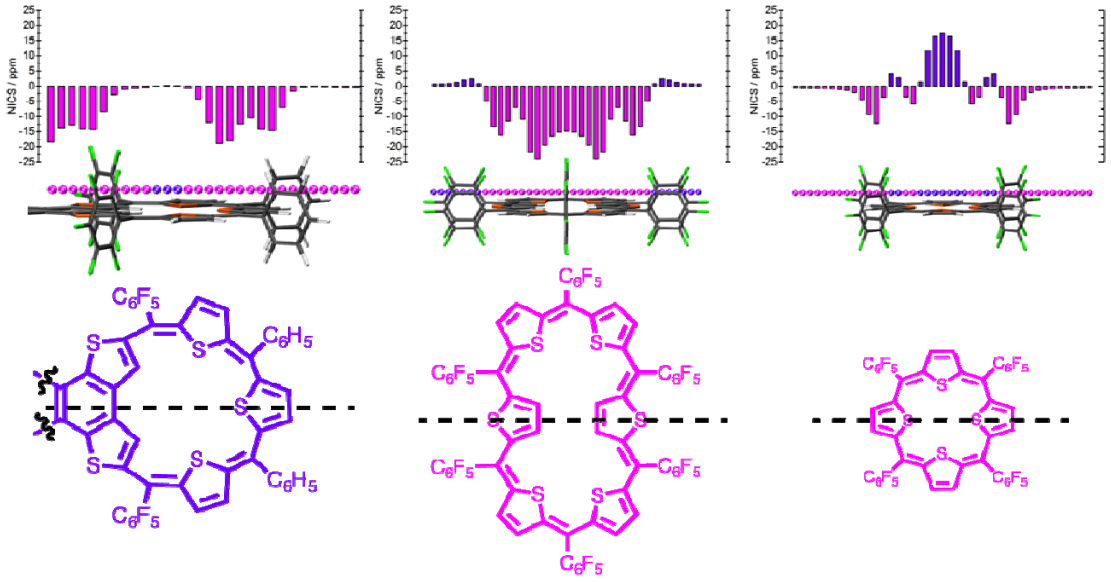

Figure S17. Calculated NICS(1) values for **6**, **S6** (down the short molecular axis), and tetra(perfluoro)phenylthiaisophlorin, with shielding values denoted in magenta and deshielding values denoted in violet.

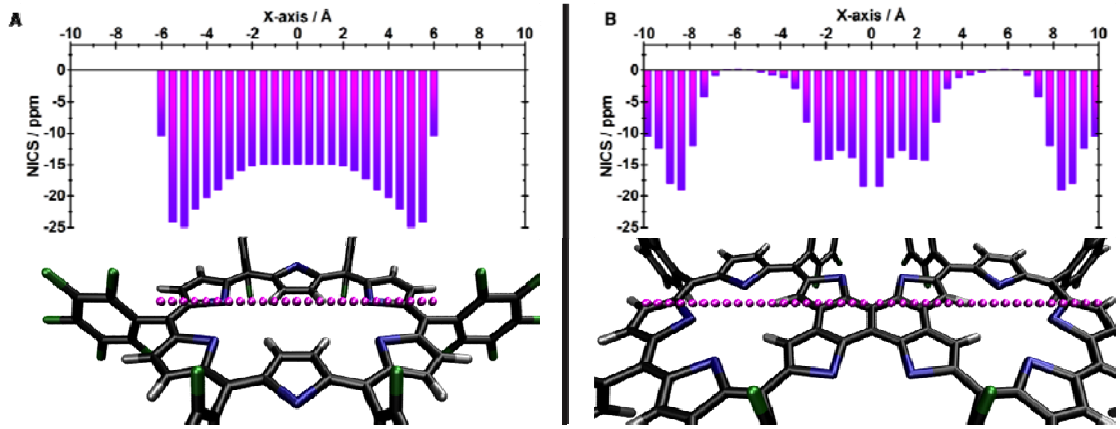

Figure S18. Calculated NICS(1) values for **S6** (down the long molecular axis) and **6**.

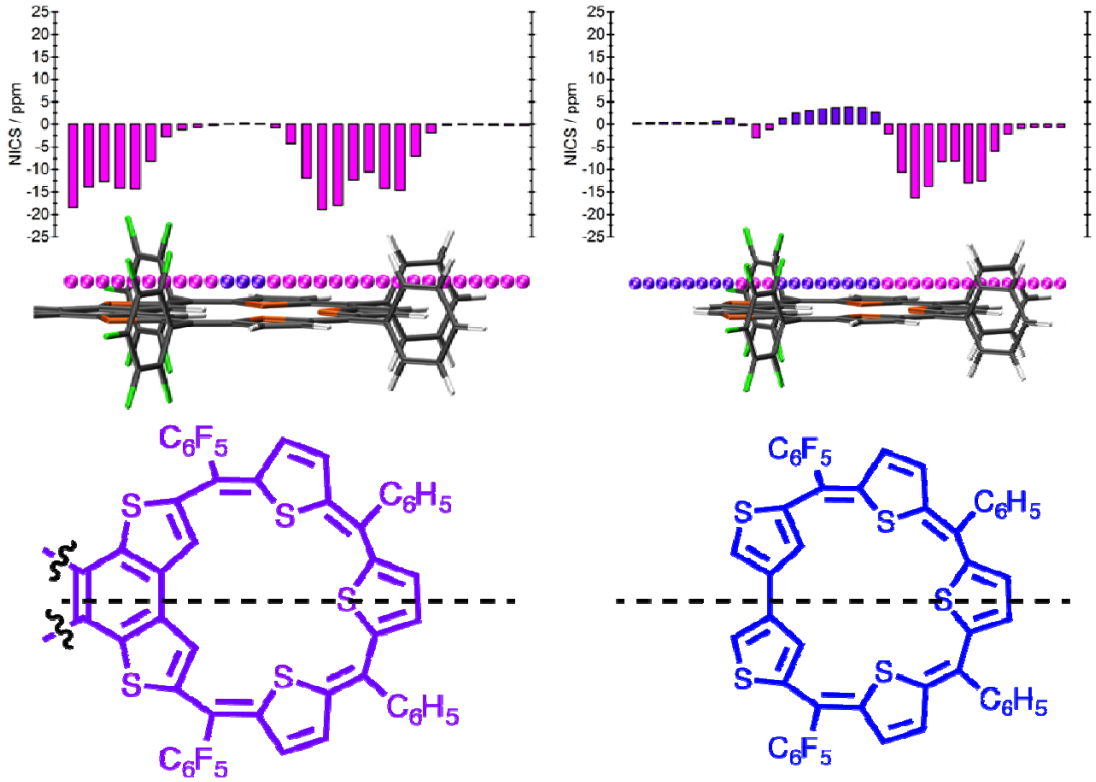

Figure S19. Calculated NICS(1) values for **6** and for the putative thiasapphyrin **7**, with shielding values denoted in magenta and deshielding values denoted in violet.

Correlation Diagram

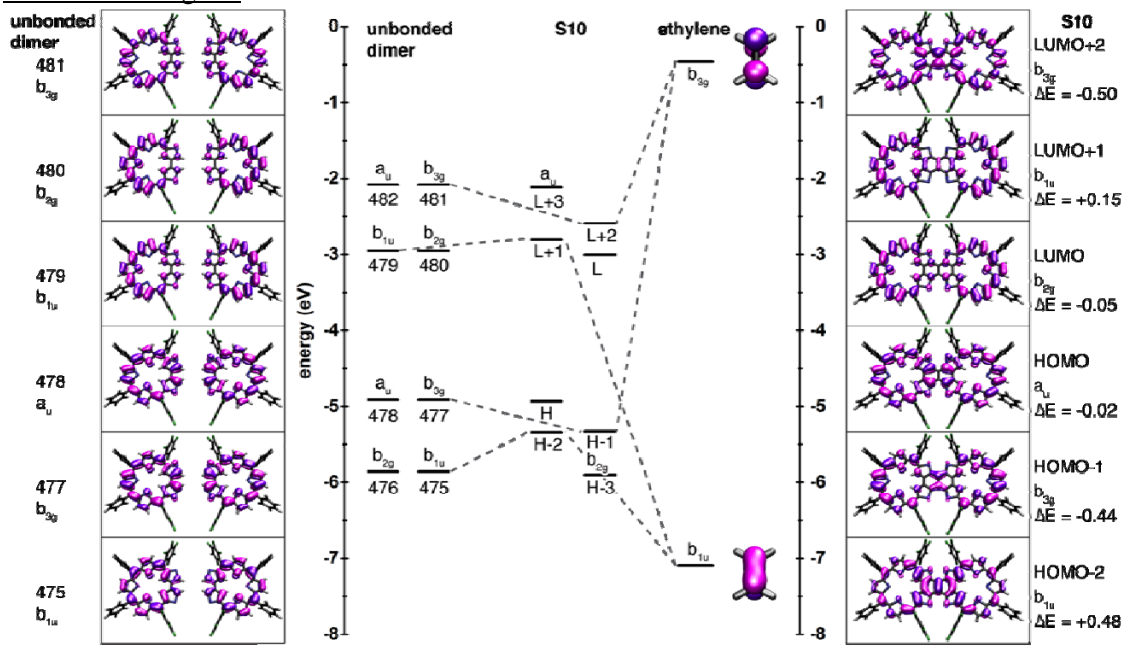

Figure S20. Expanded correlation diagram that depicts the deconstruction of the **6** compound into two thiasapphyrinoids and ethylene. All wavefunctions are plotted as 0.02 isodensity surfaces, except for those of ethylene which are 0.1 isodensity surfaces.

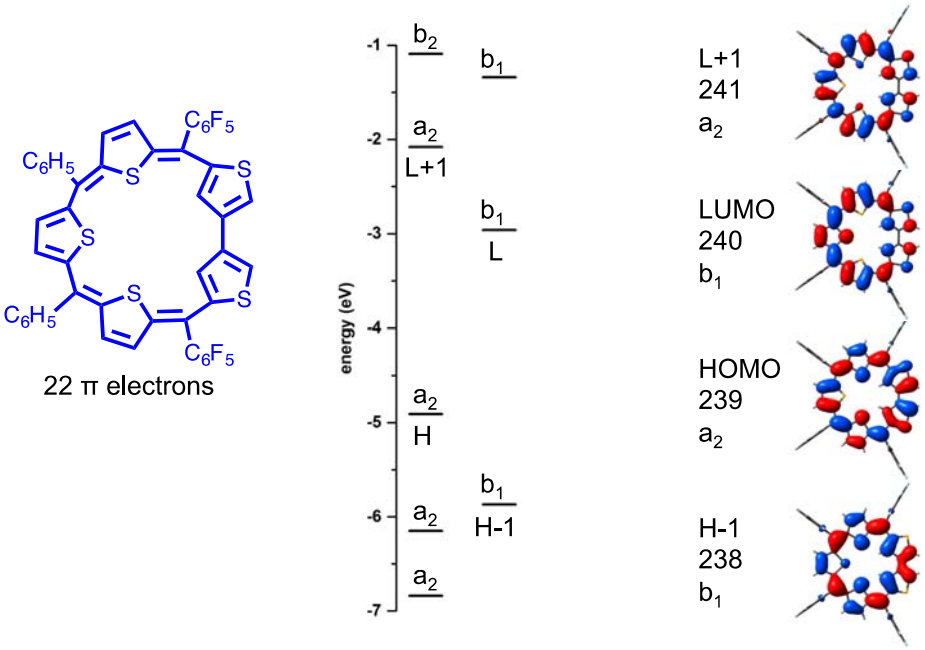

Figure S21. Thiasapphyrinoid structure **7** that constitutes the putative monomer of the **6** dimer, with its frontier orbital energy levels charted and their wavefunctions plotted as 0.02 isodensity surfaces.

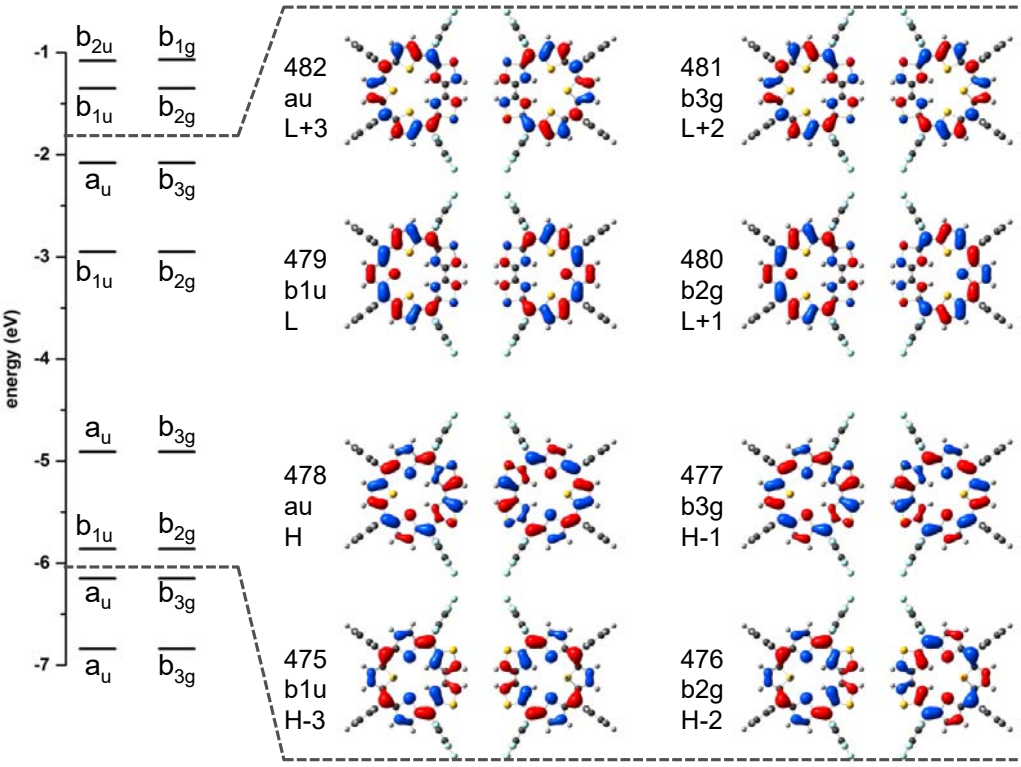

Figure S22. Expansion of the frontier orbital energy levels of the nonbonded dimer of **7**, with wavefunctions plotted as 0.02 isodensity surfaces.

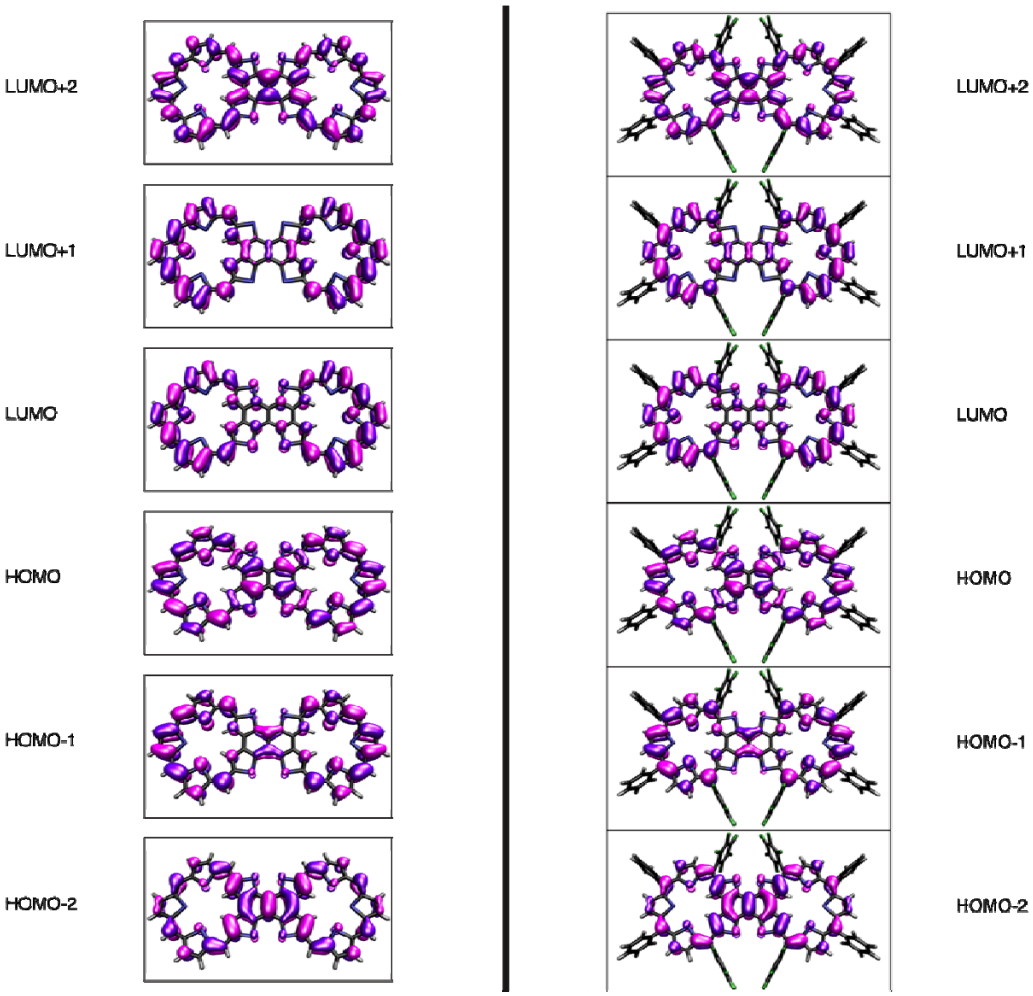

Figure S23. Qualitative comparison of the frontier orbital wavefunctions plotted as 0.02 isodensity surfaces shows that removal of the (perfluoro)phenyl rings from the **6** structure perturbs their topologies minimally. The **6** skeleton structure was used for LOL_{π} calculations.

Additional Discussion

Exciton coupling model

The spectral positions and intensities of the **6** *B*- and *Q*-bands may be further tied to transitions localized upon each of its two rings by modeling the putative thiasapphyrin monomer using TDDFT calculations, with coordinates taken from the optimized **6** structure. For this molecule, a single configuration Q_Y transition (813 nm, f = 0.15) and a weak B_Y transition dominated by H–2→L character (448 nm, f = 0.17) are predicted, 0.049 and 0.236 eV to the blue of the corresponding **6** transitions, respectively. A mixed configuration Q_X transition (521 nm, f = 0.0075) and intense multiconfigurational B_X transition (429 nm, f = 2.00) are calculated to fall 0.469 and 0.739 eV, respectively, to the blue of the corresponding **6** transitions.

The exciton coupling model[16] has provided useful insights into the major spectroscopic features of π-conjugated multiporphyrins,[17] although it was originally conceived to describe paired chromophores in the weak coupling limit. In the context of this model, the union of two thiasapphyrins engenders couplings of the transitions evinced by the monomers that shift their spectroscopic energies by magnitudes corresponding to their intensities. Thus, the relatively weak Y-polarized thiasapphyrin transitions are insufficiently blue-shifted by excitonic coupling to offset the diminution of the HOMO–LUMO gap due to dimerization. The relatively intense X-polarized transitions are strongly redshifted since their dipoles are aligned with the axis connecting the monomer chromophores. The vanishing intensity of the **6** Q_X transition, as compared to the massive long axis-polarized *Q*-derived transitions of aforementioned conjugated multiporphyrins, signifies that the two thiasapphyrinoid Q_X transition dipoles are prevented from overlapping by the break in conjugation between the rings. In sum, joining the two monomers that comprise **6** by the cross-conjugated linker stabilizes selected orbitals, holds the individual chromophores in a fixed orientation to permit their through-space interaction, but does not afford the HOMO destabilization or LUMO stabilization through extension of conjugation that would give rise to high oscillator strength in the NIR.

NICS(1) of thiasapphyrinoid **7**

NICS(1) calculations that model the ring-current shieldings of the putative thiasapphyrinoid monomer further underscore the determinative influence of this subunit on the **6** electronic structure (Figure S19). Like **6**, the monomer features local negative (shielding) values above the thiophene rings and low magnitude positive (deshielding) values in the vacancy, with a value of 3.85 ppm at the centroid. This doubly S-confused thiasapphyrin is thus predicted to exhibit a marginal global antiaromaticity, comparable with the macrocyclic aromaticity of **6**.

References

[1] E. Fischer, J. Larsen, J. B. Christensen, M. Fourmigué, H. G. Madsen, N. Harrit, *The Journal of Organic Chemistry* **1996**, *61*, 6997.

[2] J. Sreedhar Reddy, V. G. Anand, *Chemical Communications* **2008**, 1326.

[3] Z. Chen, C. S. Wannere, C. Corminboeuf, R. Puchta, P. v. R. Schleyer, *Chemical Reviews* **2005**, *105*, 3842.

[4] M. J. Frisch, G. W. Trucks, H. B. Schlegel, G. E. Scuseria, M. A. Robb, J. R. Cheeseman, G. Scalmani, V. Barone, B. Mennucci, G. A. Petersson, H. Nakatsuji, M. Caricato, X. Li, H. P. Hratchian, A. F. Izmaylov, J. Bloino, G. Zheng, J. L. Sonnenberg, M. Hada, M. Ehara, K. Toyota, R. Fukuda, J. Hasegawa, M. Ishida, T. Nakajima, Y. Honda, O. Kitao, H. Nakai, T. Vreven, J. A. Montgomery, J. E. Peralta, F. Ogliaro, M. Bearpark, J. J. Heyd, E. Brothers, K. N. Kudin, V. N. Staroverov, R. Kobayashi, J. Normand, K. Raghavachari, A. Rendell, J. C. Burant, S. S. Iyengar, J. Tomasi, M. Cossi, N. Rega, J. M. Millam, M. Klene, J. E. Knox, J. B. Cross, V. Bakken, C. Adamo, J. Jaramillo, R. Gomperts, R. E. Stratmann, O. Yazyev, A. J. Austin, R. Cammi, C. Pomelli, J. W. Ochterski, R. L. Martin, K. Morokuma, V. G. Zakrzewski, G. A. Voth, P. Salvador, J. J. Dannenberg, S. Dapprich, A. D. Daniels, Ö. Farkas, J. B. Foresman, J. V. Ortiz, J. Cioslowski, D. J. Fox, Wallingford CT, **2009**.

[5] R. Dennington, T. Keith, J. Millam, Semichem Inc., Shawnee Mission, KS, **2009**.

[6] N. M. O'Boyle, A. L. Tenderholt, K. M. Langner, *Journal of Computational Chemistry* **2008**, *29*, 839.

[7] W. Humphrey, A. Dalke, K. Schulten, *J Mol Graph* **1996**, *14*, 33.

[8] H. L. Schmider, A. D. Becke, *Journal of Molecular Structure: THEOCHEM* **2000**, *527*, 51.

[9] T. Lu, F. Chen, *Journal of Computational Chemistry* **2012**, *33*, 580.

[10] J. S. Reddy, V. G. Anand, *Journal of the American Chemical Society* **2009**, *131*, 15433.

[11] T. Yanai, D. P. Tew, N. C. Handy, *Chemical Physics Letters* **2004**, *393*, 51.

[12] a) R. C. Binning, L. A. Curtiss, *Journal of Computational Chemistry* **1990**, *11*, 1206; b) J.-P. Blaudeau, M. P. McGrath, L. A. Curtiss, L. Radom, *The Journal of Chemical Physics* **1997**, *107*, 5016; c) L. A. Curtiss, M. P. McGrath, J.-P. Blaudeau, N. E. Davis, J. R. C. Binning, L. Radom, *The Journal of Chemical Physics* **1995**, *103*, 6104; d) P. J. Hay, *The Journal of Chemical Physics* **1977**, *66*, 4377; e) R. Krishnan, J. S. Binkley, R. Seeger, J. A. Pople, *The Journal of Chemical Physics* **1980**, *72*, 650; f) A. D. McLean, G. S. Chandler, *The Journal of Chemical Physics* **1980**, *72*, 5639; g) K. Raghavachari, G. W. Trucks, *The Journal of Chemical Physics* **1989**, *91*, 1062; h) A. J. H. Wachters, *The Journal of Chemical Physics* **1970**, *52*, 1033.

[13] R. Peverati, D. G. Truhlar, *The Journal of Physical Chemistry Letters* **2011**, *2*, 2810.

[14] A. D. Becke, *The Journal of Chemical Physics* **1993**, *98*, 5648.

[15] a) C. Lee, W. Yang, R. G. Parr, *Physical Review B* **1988**, *37*, 785; b) B. Miehlich, A. Savin, H. Stoll, H. Preuss, *Chemical Physics Letters* **1989**, *157*, 200.

[16] M. Kasha, H. R. Rawls, M. A. El-Bayoumi, *Pure Appl. Chem.* **1965**, *11*, 371.

[17] a) H. L. Anderson, *Inorganic Chemistry* **1994**, *33*, 972; b) V. S.-Y. Lin, S. G. DiMagno, M. J. Therien, *Science* **1994**, *264*, 1105; c) A. Tsuda, A. Osuka, *Science* **2001**, *293*, 79; d) D. Beljonne, G. E. O'Keefe, P. J. Hamer, R. H. Friend, H. L. Anderson, J. L. Brédas, *The Journal of Chemical Physics* **1997**, *106*, 9439.